Available online at www.sciencedirect.com
ScienceDirect
Reactive & Functional Polymers 66 (2006) 1670–1683
REACTIVE & FUNCTIONAL POLYMERS
www.elsevier.com/locate/react

Electrochemical oxidative polymerization of sodium 4-amino-3-hydroxynaphthalene-1-sulfonate and structural characterization of polymeric products

G. Ćirić-Marjanović [a,*], M. Trchová [b], P. Matějka [c], P. Holler [b], B. Marjanović [d], I. Juranić [e]

[a] *Faculty of Physical Chemistry, University of Belgrade, Studentski trg 12-16, P.O. Box 137, 11001 Belgrade, Serbia*
[b] *Institute of Macromolecular Chemistry, Academy of Sciences of the Czech Republic, Heyrovský Sq. 2, 162 06 Prague 6, Czech Republic*
[c] *Department of Analytical Chemistry, Institute of Chemical Technology, Technická 5, 166 28, Prague 6, Czech Republic*
[d] *Centrohem, Karađorđeva 129, 22300 Stara Pazova, Serbia*
[e] *Faculty of Chemistry, University of Belgrade, Studentski trg 12-16, P.O. Box 158, 11001 Belgrade, Serbia*

Received 20 April 2005; received in revised form 9 June 2006; accepted 6 July 2006
Available online 17 August 2006

Abstract

The new semiconducting, electroactive, water-soluble polymeric material has been synthesized by the electrochemical polymerization of sodium 4-amino-3-hydroxynaphthalene-1-sulfonate (AHNSA–Na salt), from its aqueous solution. The polymeric products were characterized by gel permeation chromatography (GPC), conductivity measurements, cyclic voltammetry, and UV–visible, FTIR, Raman, NMR (^{1}H and ^{13}C) and electron spin resonance (ESR) spectroscopic techniques. GPC profile evidenced chains of molecular weights up to ~6300, and revealed oligomers (8-mer to 12-mer) as predominant species. FTIR spectroscopy findings of newly formed substitution patterns on naphthalene rings in the poly(AHNSA–Na salt) are well correlated with main coupling modes theoretically predicted by MNDO-PM3 semi-empirical quantum mechanical calculations. Based on these studies, it has been found that the poly(AHNSA–Na salt) consists mainly of dimer units formed *via* N–C6 and N–C8 coupling reactions. The paramagnetic nature of the poly(AHNSA–Na salt) has been proved by ESR spectroscopy, and its redox activity was confirmed by cyclic voltammetry. Intensity ratio of two new bands in the UV–visible spectrum assigned to the poly(AHNSA–Na salt) polaronic and bipolaronic forms, and the presence of naphthoiminoquinonoid and benzenoid segments detected by FTIR and Raman spectroscopy, indicate prevalence of partly and fully oxidized bipolaronic forms of the poly(AHNSA–Na salt).
© 2006 Elsevier B.V. All rights reserved.

Keywords: Electrochemical polymerization; Poly(sodium 4-amino-3-hydroxynaphthalene-1-sulfonate); Coupling mode; Redox form

Author's personal copy

1. Introduction

In the last two decades, there have been many reports which describe the electropolymerization of condensed aromatic amines, such as 1-amino-

* Corresponding author. Tel./fax: +381 11 187 133.
E-mail address: gordana@ffh.bg.ac.yu (G. Ćirić-Marjanović).

1381-5148/$ - see front matter © 2006 Elsevier B.V. All rights reserved.
doi:10.1016/j.reactfunctpolym.2006.07.002

naphthalene, 1-aminoanthracene, 1-aminopyrene and their numerous functional derivatives, in eutectic mixtures [1], nonaqueous [2–4] and aqueous media [5] on different working electrodes [6,7]. Polymeric film electrodes obtained by electrochemical oxidation of condensed aromatic amines have been the subject of investigations in the field of chemically modified electrodes because of their promising physical and chemical characteristics and potential applications in electrocatalysis [8], chemical sensor technology [9], and electrochromic display devices [10,11]. Polymer films of condensed aromatic amines were also proposed for corrosion protection of iron [12], mild steel [13], and for removal of toxic chromate ions [14]. Contrary to these enormous efforts to get as adherent as possible polymeric films of condensed aromatic amines for various useful applications, we have focused on the possibility to prepare water-soluble forms of these polymeric materials. The sodium salt of AHNSA, known as an important intermediate for the synthesis of textile dyes, looks as a promising monomer for these purposes.

It is known that introduction of sulfonic acid group as a substituent in polymeric chains of aromatic amines considerably improved their solubility in common polar solvents [15]. The aqueous medium is now mostly required in the industry because of environmental restrictions. We have supposed that sulfonic acid group in salt form will greatly enhance the solubility and work-up of AHNSA polymeric products in water, comparing with other substituted 1-aminonaphthalenes. It was expected that phenol group of AHNSA will act in a known manner [16] as a secondary self-dopant.

Besides mentioned practical aspects, oxidative polymerization of the AHNSA is interesting theoretically. Because the *para*- and *ortho*-positions to the amino group are occupied, possibility of the polymerization of AHNSA–Na salt can be questioned. Based on our previous structural characterization and stereochemical investigations of the electrochemically synthesized poly(1-aminonaphthalene) [4] and poly(2-methyl-1-aminonaphthalene) [17], we have expected that polymerization of AHNSA–Na salt will take place through possible N–C coupling reactions, where C atoms belong to the fused benzene ring that was originally without the functional groups.

In comparison with the chemical oxidative polymerization methods, the electrochemical synthesis of poly(AHNSA–Na salt) has no tricky separation of polymeric products and oxidant by-products, both being water-soluble. Trying to perform the simplest synthetic route, we have investigated electrolysis of AHNSA–Na salt without separation of the anodic and cathodic compartments. Thanks to excellent solubility of AHNSA–Na salt in water there was no need for supporting electrolyte.

To our best knowledge, there is no report relating to the electrochemical synthesis of a homopolymer of 4-amino-3-hydroxynaphthalene-1-sulfonic acid and its salts. Only copolymer of AHNSA and aniline was mentioned in the literature [18]. The aim of present work was to polymerize AHNSA–Na salt electrochemically from its aqueous solution, and to study structure of obtained polymeric products by GPC, UV–visible, FTIR, Raman, NMR and ESR spectroscopy. In addition, in this work, based on the results of spectroscopic investigations and semi-empirical quantum chemical calculations we propose the mechanism of the AHNSA–Na salt electropolymerization.

2. Experimental

The monomer, 4-amino-3-hydroxynaphthalene-1-sulfonic acid (AHNSA), (Lachema, p.a.) was used without further purification. Because of its poor solubility in water, it was transformed *in situ* in its sodium salt adding equimolar quantity of 1 mol dm^{-3} NaOH (Scheme 1).

The electrochemical instrumentation involves a PAR model 273 potentiostat/galvanostat with a thermostated three-electrode cell. The working electrode was a platinum plate of 1.6 cm^2 working area, which was heated in a reducing propane/butane flame and polished by fine emery paper No. 1200 before use. Saturated calomel electrode (SCE) was used as a reference electrode, and the counter electrode was a platinum foil.

The electrochemical oxidative polymerization was performed at a constant potential of 1.0 V vs. SCE during 10 h, at a temperature of 45 °C, using 0.084 mol dm^{-3} aqueous solution of the AHNSA–

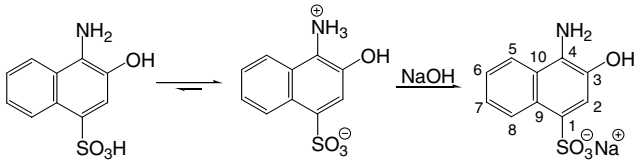

Scheme 1. Preparation of the sodium 4-amino-3-hydroxynaphthalene-1-sulfonate in aqueous solution.

Author's personal copy

Na salt (10 ml of this solution) without adding any supporting electrolyte. By evaporation of exhaustively electrolyzed solution, a black-violet product – poly(AHNSA–Na salt) was obtained which was dried under vacuum for 2 h at 50 °C.

Electrochemical properties of the 0.084 mol dm^{-3} AHNSA–Na salt solution at the beginning of the reaction and after 10 h of the electropolymerization at a constant potential were studied by cyclic voltammetry in the potential range from −0.9 V to 1.0 V vs. SCE at a sweep rate of 50 mV s^{-1}.

Molecular weights of poly(AHNSA–Na salt) were assessed with the gel permeation chromatography using 500 × 8 mm Labio GM 1000 column operating with *N*-methyl-2-pyrrolidone and calibrated with polystyrene standards, using toluene as an internal standard and spectrophotometric detection at a wavelengths of 436 and 650 nm. The samples for GPC measurements were prepared by dissolving 10 mg of polymeric sample in 5 ml *N*-methyl-2-pyrrolidone containing 100 mg triethanolamine to deprotonate the sample and to improve its solubility. Mobile phase, *N*-methyl-2-pyrrolidone, contained 0.5% LiBr to prevent aggregation. Flow rate was 1 ml min^{-1}. GPC data were treated by CSW1.7 software and GPC for Win.

UV–visible spectra of the AHNSA–Na salt solution as well as of the poly(AHNSA–Na salt) solutions got from the reaction system during the electropolymerization were obtained with a Carl Zeiss Jena UV–VIS spectrophotometer. Concentration of the AHNSA–Na salt solutions used for UV–visible spectroscopy study of the course of polymerization was 1.0×10^{-4} mol dm^{-3}.

Infrared spectra in the range of 400–4000 cm^{-1} were recorded with a fully computerized Thermo Nicolet NEXUS 870 FTIR Spectrometer (64 scans per spectrum at 2 cm^{-1} resolution) equipped with DTGS TEC detector. Powdered samples were dispersed in potassium bromide and compressed into pellets. Spectra were corrected for the content of H_2O and CO_2 in the optical path.

Raman spectra with the excitation in the visible range at 488 nm were collected on the LabRam system (Dilor) equipped with an external Ar^+-ion laser (Melles Griot). The laser power on the head of laser was 15 mW, but a grey filter reducing the laser power of two orders of magnitude was used in all experiments, i.e. the laser power on sample did not exceed 0.15 mW. The objectives (×50, ×100) were used to focus the laser beam on the sample placed on X–Y motorized sample stage. The scattered light was analyzed by spectrograph with holographic grating (1800 lines mm^{-1}), slit width 100 μm and quite opened confocal hole (1000 μm). Peltier-cooled CCD detector (1024 × 256 pixels) detected the dispersed light. The adjustment of the system was regularly checked using a sample of silicon and by the measurement in the zero-order position of the grating. The time of acquisition of particular spectral window was optimized for individual sample measurement (from 0.1 s to 120 s). The auto-repeat function was used to monitor the time dependence of spectra. The spectrometer and the positioning of a sample were controlled via PC (Pentium, Dell) with Labspec v. 2.08 (Dilor) software. The same software was used for treatment of the data obtained.

Raman spectra with 1064 nm excitation line were collected using Bruker IFS 55 EQUINOX FTIR Spectrometer equipped with FRA 106/S Fourier Transform Raman Module with Diode-pumped, temperature-stabilized Nd YAG laser, and InGaAs detector. Optics for the collection of 180° Raman scattering (back-scattering) from powdered samples in standard sample holders was used for measurements at room temperature. The OPUS version 4 software was used for treatment of the data obtained.

^1H and ^{13}C nuclear magnetic resonance (NMR) spectra were recorded at 200/50 MHz with tetramethylsilane (TMS) as internal standard on a Varian "Gemini 200" spectrometer in DMSO-d_6. The chemical shifts are expressed as ppm downfield from TMS.

ESR measurements were obtained using Varian E104-A ESR spectrometer operating at X-band (9.51 GHz), using following settings: 100 kHz modulation frequency, 2.0 G modulation amplitude, 10 mW microwave power and 100 G scan range. Solid state samples were measured at room temperature using quartz tubes. Spectra were recorded and analyzed using EW software (Scientific Software).

The computational method used here to obtain the molecular orbitals, ionization energy, heat of formation, and spin density of the species considered is semi-empirical MNDO-PM3 model [19–21] (included in MOPAC 97, part of the Chem3D Pro 5.0 package, CambridgeSoft Corporation) with full geometry optimization, taking in account solvation in water (using COSMO facility) [22]. For the molecular structures, we have used the restricted Hartree–Fock method (RHF) and the unrestricted Hartree–Fock (UHF) method for the radical species.

Authors personal copy

For conductivity measurements, polymeric samples were pressed into pellets, 10 mm in diameter and 1 mm thick, under a pressure of 124 MPa using a hydraulic pellet press. The conductivity was measured between stainless pistons at room temperature by means of an ac bridge (Waynne Kerr Universal Bridge B 224) at fixed frequency of 1.5 kHz. During the measurement, pressure was maintained at the mentioned value.

3. Results and discussion

3.1. Electrochemical polymerization

At the beginning of the anodic oxidation process, a neutral solution is obtained (pH $\sim$ 7.0) because the AHNSA–Na is a salt of a strong acid (AHNSA) and a strong base (NaOH). The acidity of reaction solution only slightly increases, i.e. pH decreases to the pH 5.5 during the electrooxidation process, since protons formed by the anodic oxidative coupling of AHNSA–Na salt (two protons per one monomer molecule) mainly undergoes cathodic reduction. The current measured at the constant anodic potential of 1.0 V vs. SCE decreases continually from about 35 mA, at the start of the electrolysis, to about 0.8 mA after the reaction time of 10 h. During the electrolysis, color changes of reaction solution of the AHNSA–Na salt occur gradually from orange-red to violet-black. The polymerization product does not form an adhesive polymeric film at the anode and it is soluble in water. This property could be very important for the processing of synthesized poly(AHNSA–Na) and it is desirable for its various potential applications.

3.2. Gel permeation chromatography

The successful electropolymerization of the AHNSA–Na salt was clearly proved by the GPC profile of its oxidation products. The molecular weight approach the maximum value of ~6300 (Fig. 1). This result confirms our prediction that the polymerization of the AHNSA–Na salt would occur in considerable extent despite the fact that substituents at the *para*- and *ortho*-positions to the amino group blocked well-known polymerization routes of 1-aminonaphthalenes. GPC profiles showed unimodal molecular weight distributions for used detection wavelengths, λ_d, of 436 and 650 nm, which is indicative that chain branching reactions did not occur to a major extent. The

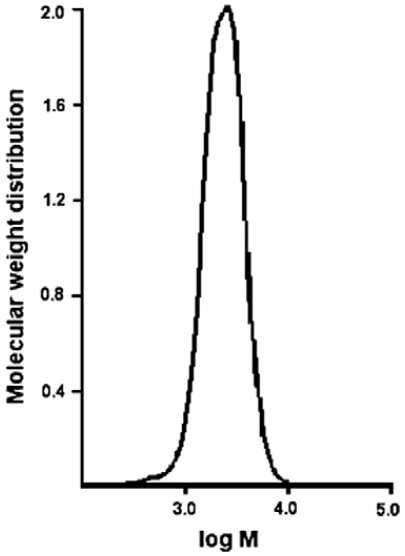

Fig. 1. Molecular weight distribution as obtained by GPC for the electropolymerization products of the AHNSA–Na salt, with spectrophotometric detection at a wavelength of 436 nm.

weight-average and number-average molecular weights, M_w and M_n, were calculated to amount 2570 and 2070 ($\lambda_d = 436$ nm), respectively, and 1770 and 1010 ($\lambda_d = 650$ nm), respectively. The polydispersity (M_w/M_n) values are 1.24 ($\lambda_d = 436$ nm) and 1.75 ($\lambda_d = 650$ nm), indicating a relatively narrow molecular weight distribution of the AHNSA–Na salt polymeric products. GPC measurements revealed oligomers (8-mer to 12-mer) as predominant species.

3.3. FTIR spectroscopy

The comparative study of the AHNSA and poly(AHNSA–Na salt) FTIR spectra in the low-frequency region 650–1000 cm^{-1} (Fig. 2), corresponding to the aromatic C–H out-of-plane deformation vibrations, γ(C–H) [23,24], revealed changes of the aromatic substitution pattern. In the monomer spectrum two bands appear at 750 and 775 cm^{-1} due to the γ(C–H) vibrations of four adjacent hydrogen atoms of the fused benzene ring without functional groups, Table 1. The disappearance of these bands accompanied with the appearance of new bands at 725 and 760 cm^{-1} in the spectrum of poly(-AHNSA–Na salt) corresponds well to the formation of trisubstitution pattern with three adjacent H atoms [23–25], which is indicative for the coupling reactions at the C5 (C8) positions of the AHNSA naphthalene ring. The trisubstitution pattern with one isolated and two adjacent H atoms, corresponding to the coupling reactions at the C6 (C7) positions,

Author's personal

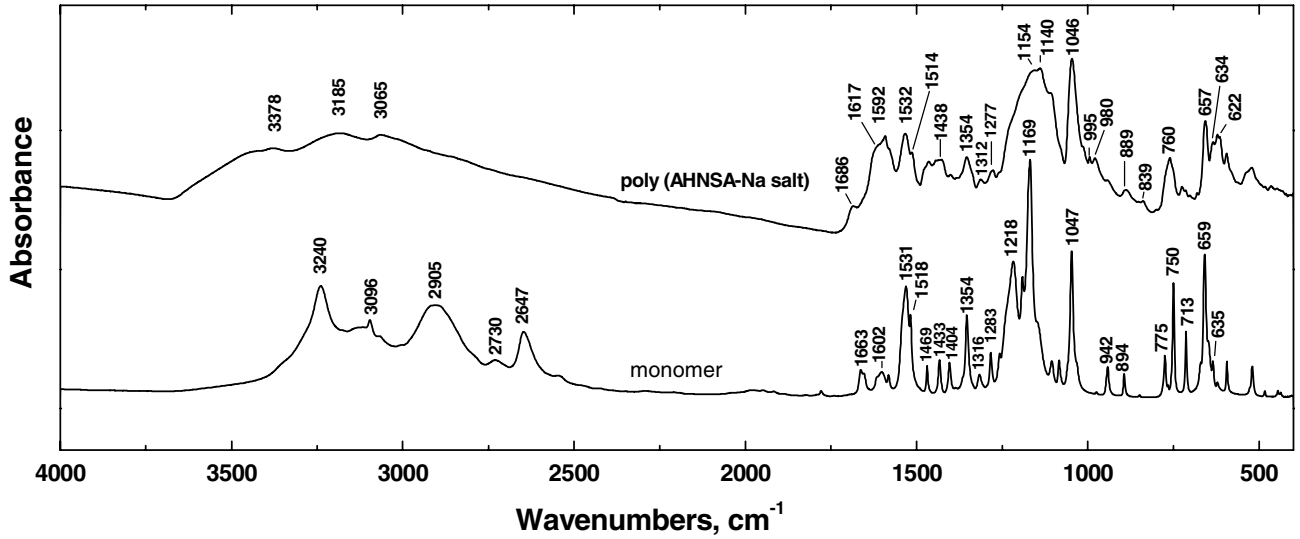

Fig. 2. FTIR spectra of AHNSA and poly(AHNSA–Na salt) synthesized electrochemically.

Table 1
FTIR bands of AHNSA and poly(AHNSA–Na salt) and their assignment

Wavenumber (cm^{-1})		Assignment
AHNSA	Poly(AHNSA–Na salt)	
775 m		γ(C–H) (4 adjacent H in the disubstituted benzene ring)
	760 m	γ(C–H) (3 adjacent H in the trisubstituted benzene ring)
750 s		γ(C–H) (4 adjacent H in the disubstituted benzene ring)
	839 w	γ(C–H) (2 adjacent H in the trisubstituted benzene ring)
	725 w-m	γ(C–H) (3 adjacent H in the trisubstituted benzene ring)
894 w	889 w	γ(C–H) (1 isolated H in the pentasubstituted benzene ring)
	980 m, 995 m	C–H in-plane def. in the trisubstituted benzene ring
1047 s	1046 vs	Symmetric stretching of SO_3 group
1169 vs	1154 vs, br	Asymmetric stretching of SO_3 group
1218 s	1218 sh	C–O stretching of phenols
1316, 1283	1312, 1277	C–N stretching of aromatic amines
1354 m	1354 m	O–H in-plane bending
1531, 1518, 1469	1532, 1514, 1475, 1464	C–C stretching in benzenoid ring
	1592 s, br	C═C stretching in naphthoiminoquinonoid ring
	1685 w-m	C═O stretching in naphthoiminoquinonoid ring
3096	3065	Aromatic C–H stretching
3240	3185	Hydrogen-bonded O–H and N–H stretching
3350	3440, 3378	N–H stretching of aromatic amine

Author's personal

is revealed by the band at 839 cm^{-1} in the poly-(AHNSA–Na salt) spectrum, due to the γ(C–H) vibration of two adjacent ring H atoms [23,26]. In accordance with these findings, two new bands at 980 and 995 cm^{-1} in the spectrum of polymeric product are attributable to the aromatic C–H in-plane deformation vibrations of the trisubstituted benzene rings with three adjacent H atoms, or/and with one isolated and two adjacent H atoms [23]. The appearance of the band at 889 cm^{-1} in the poly (AHNSA–Na salt) spectrum suggests that pentasubstitution pattern of the fused benzene ring bearing functional groups, evidenced by the γ(C–H) band at 894 cm^{-1} in the monomer spectrum, remains unchanged in the polymerization product [23,26].

In the 1000–1700 cm^{-1} region of the poly (AHNSA–Na salt) FTIR spectrum (Table 1), the new band at 1685 cm^{-1} could be attributed to the stretching vibration of the carbonyl group of naphthoiminoquinonoid ring [25]. The new strong band at 1592 cm^{-1} and its shoulder at 1617 cm^{-1} correspond to the C═C stretching [12,27,28] and the C═N stretching vibrations of naphthoiminoquinonoid ring [23], respectively. The bands observed at

1532, 1514, 1475 and 1464 cm^{-1} in the polymer spectrum are assigned to C–C benzenoid ring stretching vibrations [12,25,28–30]. The C–N stretching of aromatic amines is evidenced by two bands at 1312 cm^{-1} and 1277 cm^{-1} in poly(-AHNSA–Na salt) spectrum [12,25]. The strong band observed at 1218 cm^{-1} in the monomer spectrum corresponds to the stretching C–O vibration of phenols [25,31]. In the poly(AHNSA–Na salt) FTIR spectrum, this band is observable as a shoulder of the band at 1154 cm^{-1}. The presence of the band at 1354 cm^{-1}, attributable to the phenol O–H in-plane bending vibration, in the monomer and poly(AHNSA–Na salt) spectra [25,26,31], suggests that this group does not take part in a coupling reactions during polymerization process. The dominant bands in the polymer spectrum due to the asymmetric and symmetric stretching vibrations of sulfonate group are detected at 1154 and 1046 cm^{-1}, respectively [26].

Observed band broadening in the region 3570–3200 cm^{-1} reflects the organization of polymeric chains by hydrogen bonding, involving aromatic amine NH and phenolic OH as a donors of $H^{\delta+}$, and aromatic amine NH, phenolic OH, naphthoiminoquinonoid C=O and C=N groups as $H^{\delta+}$ acceptors [25,32,33].

3.4. Quantum chemical calculations

Semi-empirical quantum mechanical calculations and the frontier orbital method are reliable in the prediction of molecular structure [34] and stereochemistry [4] of conductive polymers. It is proposed

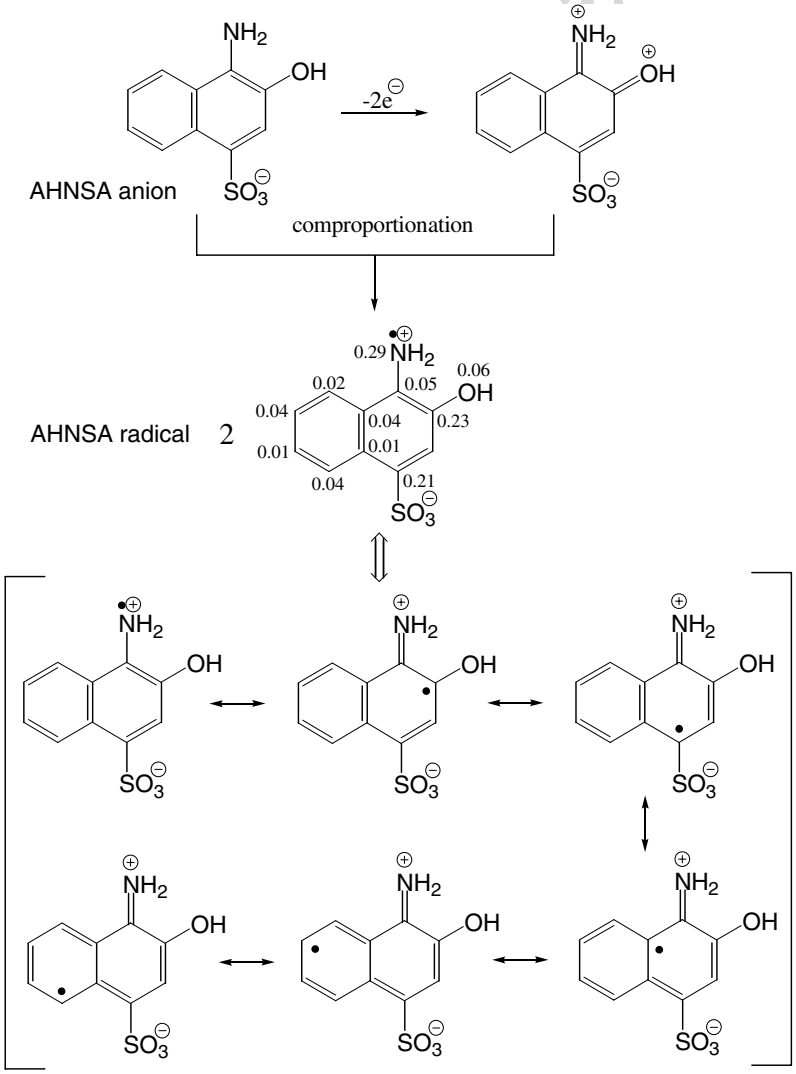

Scheme 2. Total spin density of the hydrated dipolar ion radical formed from AHNSA anion, computed by PM3 RHF hamiltonian after PM3 UHF optimization of geometry. The resonance canonical forms of the AHNSA radical are also shown.

by many authors that the initial step of the electrochemical oxidative polymerization of aromatic amines is the generation of their cation radicals. As in the case of the anodic oxidation of the 4-aminodiphenylamine [35], we propose that the AHNSA radicals are generated *via* comproportionation reaction between AHNSA–Na salt and its oxidized form obtained by two-electron oxidation, rather than by the one-electron anodic oxidation of the monomer (Scheme 2). This is confirmed by the significant decrease of ionization energy, i.e. the increase of the oxidizability of hydrated AHNSA radical ($E_i = 5.36$ eV) compared with hydrated AHNSA anion ($E_i = 8.60$ eV). The PM3 computations revealed increase of the electric dipole moment of generated radical (25.7 D) compared with the hydrated AHNSA anion (18.3 D). This dipole increment is consistent with the dipolar ionic nature of

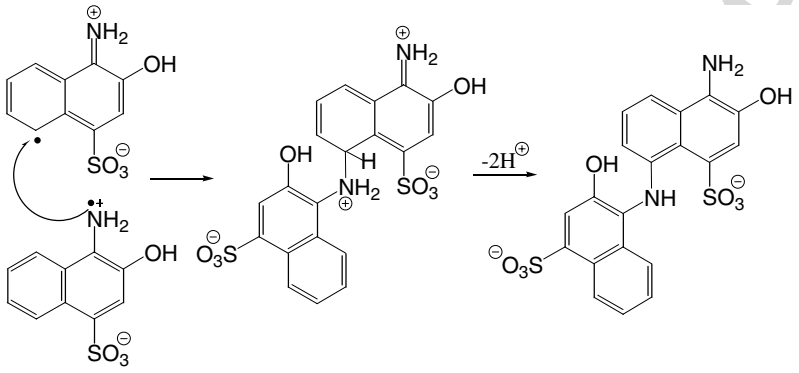

Scheme 3. The proposed polymerization mechanism of AHNSA–Na salt shown for N–C8 coupling reaction.

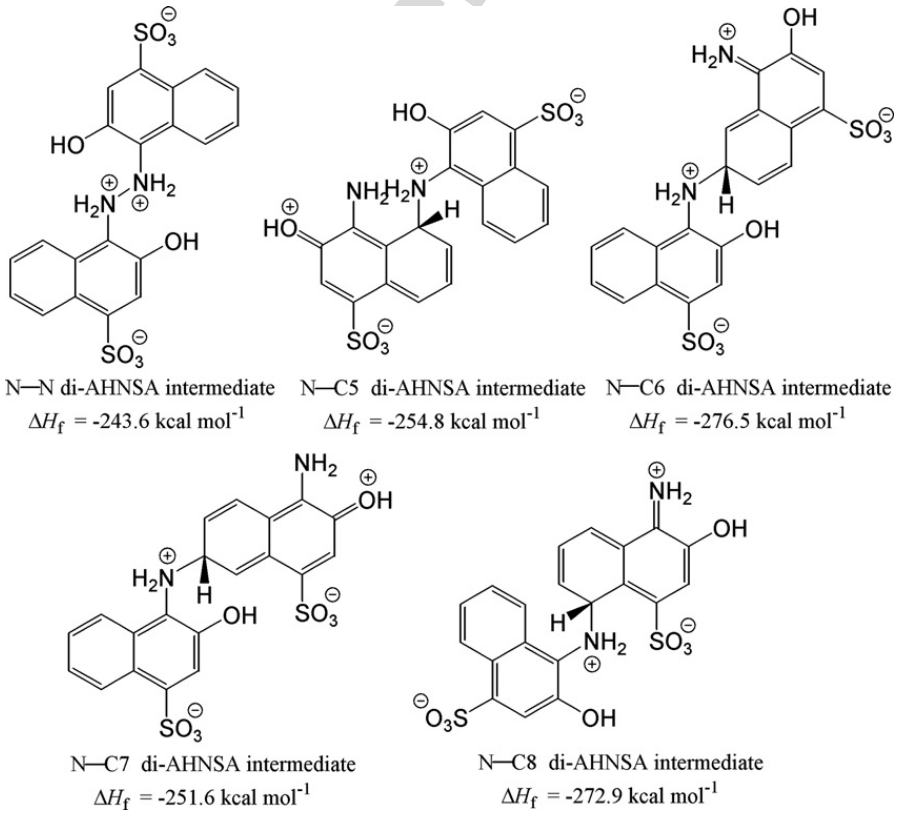

Scheme 4. Heat of formation ΔH_f of hydrated di-AHNSA intermediates formed *via* N–N, N–C5, N–C6, N–C7 and N–C8 coupling reactions, computed by the PM3 RHF method.

generated AHNSA radical, expressed well by its resonance hybrid form (Scheme 2).

Molecular orbital MNDO-PM3 computations show that the SOMO of the hydrated AHNSA radical is delocalized mainly over the substituted fused benzene ring (excluding C2 and C9) and the nitrogen. The major part of the spin density is associated with the nitrogen (0.29), the C1 (0.21) and the C3 (0.23), Scheme 2. Based on the spin density of the amino nitrogen and phenolic oxygen (0.06) it could be concluded that aromatic amine oxidative polymerization dominates over phenol oxidative polymerization, as found experimentally.

Generated *via* comproportionation redox process, the AHNSA radicals instantaneously react among themselves, and radical–radical couplings lead to dimeric intermediates. These intermediates then lose two protons, generating dimer products (Scheme 3), which are further oxidized to radicals. This allows radical–radical coupling to continue, and polymerization to progress to completion.

Computation of coupling rates of the dimerization of AHNSA–Na salt strongly depends on the interatomic distance between two atoms involved in the coupling, which remains unknown in the frontier orbital method. This is further complicated by the hydration of reactive species and especially by the influence of relative position of sodium cations to transition complex. In accordance with Hammond's postulate [36], we based our prediction of dominant AHNSA coupling reactions on the stability of the AHNSA dimeric intermediates, resembling structurally the transition state of the AHNSA radical recombination, rather than on the stability of the AHNSA dimers.

Thus, taking into account the spin density distribution of hydrated AHNSA dipolar ion radical (Scheme 2), steric repulsions during dimerization, and the heat of formation, ΔH_f, of di-AHNSA intermediates (Scheme 4) we propose N–C6 and N–C8 as the main coupling modes in the poly(-AHNSA–Na salt).

Good correlation between theoretically predicted and experimentally determined coupling modes has been found. The newly formed trisubstitution pattern with three adjacent H atoms on the fused benzene ring, as revealed by the FTIR spectroscopy study of the poly(AHNSA–Na salt) macromolecular structure, corresponds to the N–C8 linkage between AHNSA monomer units. The newly formed trisubstitution pattern with one isolated and two adjacent H atoms on the fused benzene ring could be correlated with the N–C6 coupling mode.

3.5. UV–visible spectroscopy

During the electrooxidation of the AHNSA–Na salt colored products, soluble in aqueous solution, are formed and the electropolymerization course is easily followed by UV–visible spectroscopy (Fig. 3). The aqueous solution of monomer has a low absorption without noticeable bands in the wavelength region 400–800 nm. After application of 1.0 V potential on the working electrode, two new absorption bands appeared with maxima at 480 nm and 645 nm, and a continuous growth of their intensities was observed during the electropolymerization.

We propose that bands of the poly(AHNSA–Na salt) at 645 nm and 480 nm correspond to polymeric segments of lower (polaronic form) and higher oxidation state (bipolaronic forms), respectively (Scheme 5). The spectrum of the monomer shows $\pi \rightarrow \pi^*$ transition band at 345 nm. As the AHNSA–Na salt concentration rapidly decreases on account of the initial formation of its two-electron oxidation product (Scheme 2), intensity of this band shows pronounced decrease at the start of polymerization. This band has been transformed to the $\pi \rightarrow \pi^*$ transition peak of the benzenoid moiety in the poly(AHNSA–Na salt)

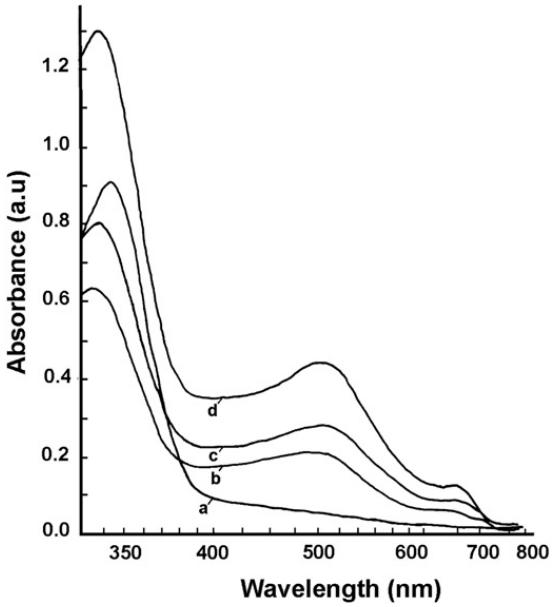

Fig. 3. UV–visible absorption spectra of the aqueous solution of AHNSA–Na salt before and during the electrochemical polymerization reaction: curve a – before the start of the electrolysis; curve b – at 372 min of the electrolysis; curve c – at 510 min of the electrolysis; curve d – at 577 min of the electrolysis.

Author's personal copy

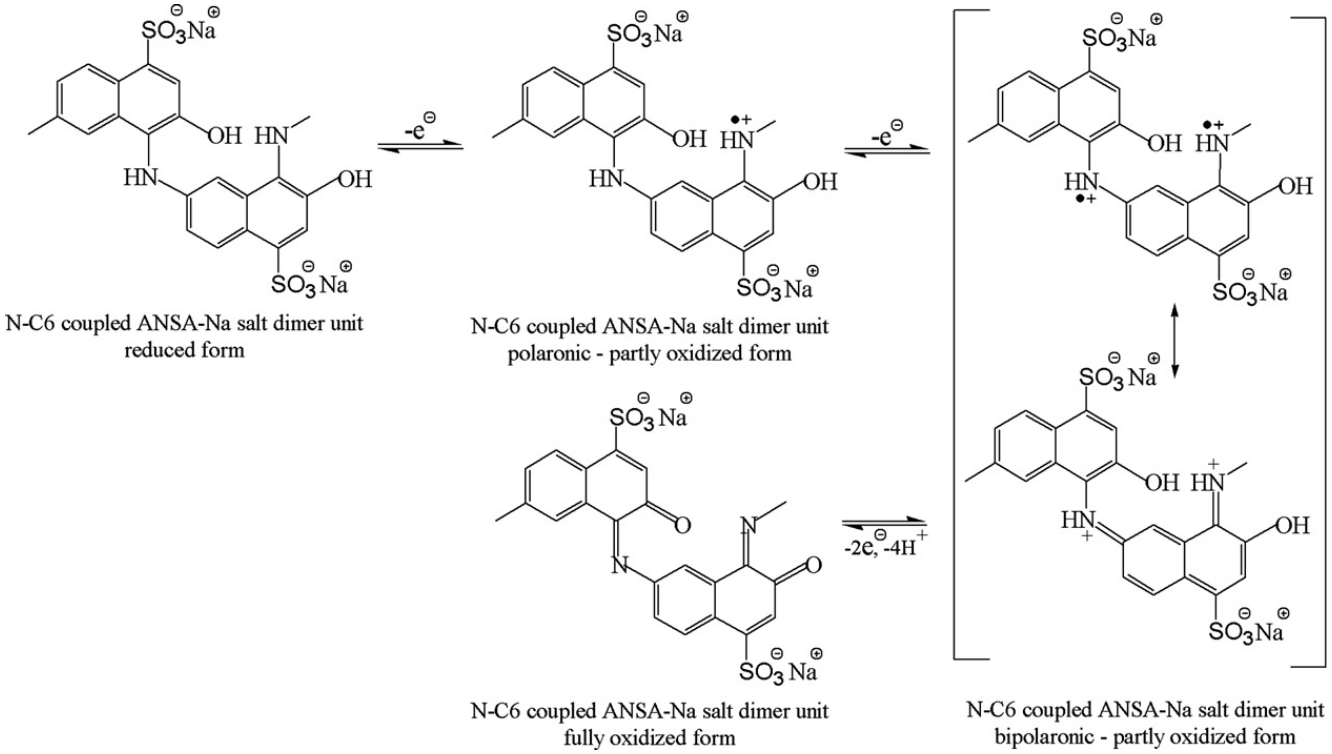

Scheme 5. Redox equilibriums of N–C6 coupled dimer units in poly(AHNSA–Na salt).

structure, positioned at 335–340 nm [28], which gradually increases during the polymerization process.

The question arises about the nature of polaronic and bipolaronic forms of the poly(AHNSA–Na salt). It is shown on the example of N–C6 coupling route (Scheme 5) that the reduced form of AHNSA–Na salt dimer unit can be oxidized by one-electron process to polaronic, like-emeraldine salt partly oxidized product. This further loses an electron, producing bipolaronic partly oxidized form, which finally, by two-electron oxidation process, give fully oxidized *ortho*-naphthoiminoquinonoid N–C6 AHNSA–Na salt dimer unit. Based on the intensity ratio of absorbance bands with maxima at 480 nm (bipolaronic) and 645 nm (polaronic), we proposed bipolaronic, partly and fully oxidized forms of the poly(AHNSA–Na salt), as dominant.

3.6. Raman spectroscopy

It is known that different excitation wavelengths can selectively enhance the intensity of the Raman bands originating from the polymeric segments differing in their oxidation state. Based on our UV–visible spectroscopic investigations of the poly(AHNSA–Na salt), which proved existence of its visible absorption bands, (Fig. 3), we have expected appearance of the resonance Raman effect for this polymeric compound. This means that bands originating from the oxidized polymeric segments should be enhanced when the frequency of the exciting radiation coincides with that of the electronic transition [28,37]. With the aim of separating the modes originating from co-existing polymeric segments of various oxidation states, we exploited Raman spectroscopy in visible (excitation wavelength $\lambda_{exc} = 488$ nm) and NIR ($\lambda_{exc} = 1064$ nm) regions for the samples of AHNSA monomer and poly(AHNSA–Na salt), Fig. 4.

In the Raman spectrum of the monomer for $\lambda_{exc} = 1064$ nm, bands at 1214 and 1250 cm^{-1} are observable. These bands are shifted to the positions of 1215 and 1240 cm^{-1} in the spectrum of poly(AHNSA–Na salt) for the same excitation line, and are attributable to the C–N stretching and benzenoid ring deformation vibrations, respectively [38]. In the monomer and polymer spectra for $\lambda_{exc} = 488$ nm only one band located at 1230 and 1220 cm^{-1}, respectively, is observed. This band is assigned to the C–N stretching vibration [39].

The band located at 1320 cm^{-1} is observed for $\lambda_{exc} = 1064$ nm in the spectrum of monomer, attributable to the C–N stretching vibration, while in the spectrum of polymeric product this band is shifted

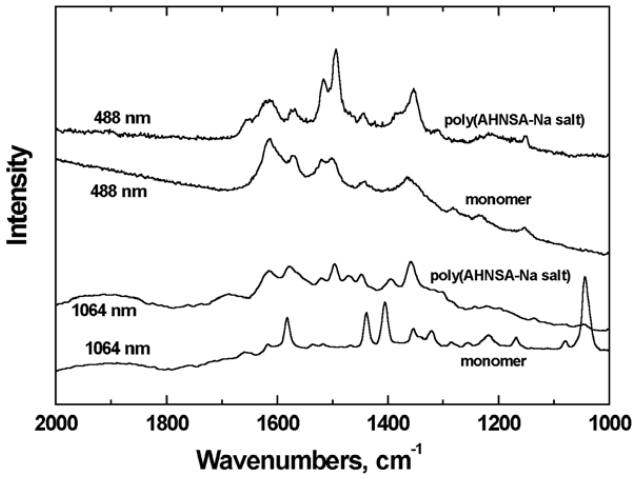

Fig. 4. Raman spectra of the AHNSA and poly(AHNSA–Na salt) synthesized electrochemically, measured by using two different excitation lines (488 nm and 1064 nm).

to the position of 1300 cm^{-1}, and could be assigned to the C∼$N^{\cdot+}$ stretching vibration of isolated polarons (localized cation radicals) [40]. For $\lambda_{exc} = 488$ nm in poly(AHNSA–Na salt) spectrum the band at 1314 cm^{-1} is observed, while in the corresponding monomer spectrum this band is not clearly observed. This band can be attributed to the C∼$N^{\cdot+}$ stretching vibration of polarons [40].

In the spectrum of the polymer, measured with $\lambda_{exc} = 1064$ nm, two bands at 1520 cm^{-1} and 1498 cm^{-1} are observed. When the excitation wavelength is changed from 1064 nm to 488 nm, these bands in the polymer spectrum are enhanced and shifted to the positions 1518 cm^{-1} and 1496 cm^{-1}, respectively. The observed resonance Raman effect suggests that these modes are related to the oxidized, bipolaronic segments in the poly(AHNSA–Na salt). These bands, corresponding to the C=N stretching mode [12,28,41,42], can originate from two different *ortho*-naphthoiminoquinonoid rings formed by the oxidation of N–C6 and N–C8 coupled AHNSA dimer units.

In the Raman spectra of the electropolymerization product, for $\lambda_{exc} = 488$ nm, we observe a weak band about 1655 cm^{-1}, which is not observed in the monomer spectrum. This band can stem from the carbonyl group of *ortho*-naphthoiminoquinonoid rings. The band at 1617 cm^{-1} is present in all spectra of monomer and polymeric samples. It is attributable to the mode of C∼C stretching vibration of the benzenoid ring [28,41]. The strong peak at 1583 cm^{-1} in the spectrum of AHNSA monomer obtained with $\lambda_{exc} = 1064$ nm is shifted to 1578 cm^{-1} in the spectrum of polymeric sample. These bands can be attributed to the C∼C stretching modes of naphthalene and *ortho*-naphthoiminoquinonoid rings, respectively.

3.7. NMR spectroscopy

As the poly(AHNSA–Na salt) is soluble in DMSO, ^{1}H and ^{13}C NMR spectroscopy study of its macromolecular structure was performed (Figs. 5 and 6). From the first glance, the ^{1}H and ^{13}C NMR spectra suggest that we are dealing with a mixture of oligomers with slightly different structures.

The signal assignment corresponds to carbon (and attached proton) numbering in Scheme 6, containing the proposed prevailing structure of poly(-AHNSA-Na salt). This proposed structure is consistent with FTIR, UV–visible, and Raman spectroscopic analysis combined with MNDO-PM3 semi-empirical quantum chemical theoretical approach.

The multiplet in the region 7.20–7.50 ppm in the ^{1}H NMR spectrum is attributed to protons attached to the C7 position of naphthalene and *ortho*-naphthoiminoquinonoid structural units (A, B, C, D), which show triplet at 7.41 ppm in the AHNSA monomer. The multiplet in the region 7.55–7.70 corresponds to protons attached to the C6 position (C, D), which show triplet at 7.56 ppm in the AHNSA. Relatively low intensity of this ^{1}H NMR signal, comparing with other signals originating from aromatic protons, indicates C6 as a preferential coupling site in the poly(AHNSA–Na salt). The multiplet in the region 7.70–8.30 could be assigned to protons attached to the C2 (7.85 ppm in the AHNSA) (A, C) and C5 (7.83 ppm in the AHNSA) positions (A, B, C, D), while the multiplet signal in the region 8.40–9.00 is attributable to the C8 attached protons (A, B), which show doublet at 8.79 ppm in the AHNSA. We propose that the low intensity singlets in the region 4.90–6.30 ppm originated from the isolated polaronic sites (–$NH^{\cdot+}$–). The broad singlet at 6.90 is well correlated with protons attached to the C2 position of the *ortho*-naphthoiminoquinonoid units (B, D). The singlets in the region 9.20–10.40 are assigned to the phenolic protons, indicating inter-macromolecular hydrogen bonding.

The ^{13}C NMR spectrum of the poly(AHNSA–Na salt), Fig. 6, clearly shows the appearance of new types of carbon atoms in the macromolecular structure, comparing with corresponding spectrum

Author's personal copy

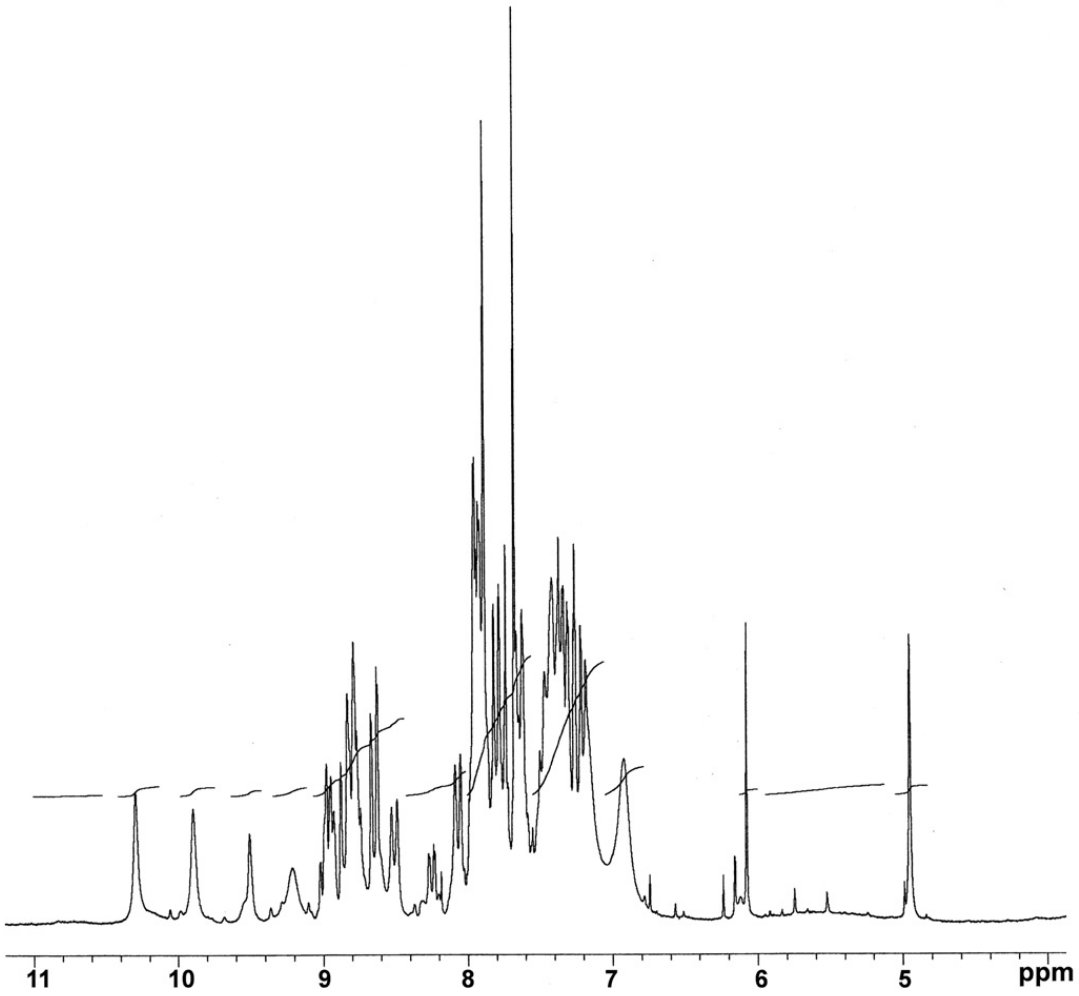

Fig. 5. The ^{1}H NMR spectrum of the poly(AHNSA-Na salt).

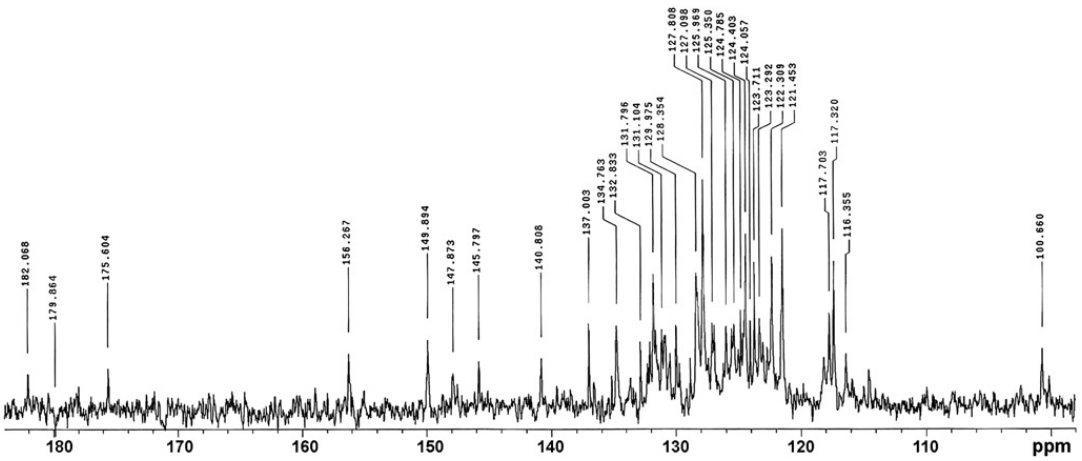

Fig. 6. The ^{13}C NMR spectrum of the poly(AHNSA-Na salt).

of monomer. New signals in the region 175–185 ppm are originated from the C3 and C4 carbon atoms of carbonyl and imino groups in the newly formed *ortho*-naphthoiminoquinonoid units (B, D). The new signal at 156 ppm corresponds to the C1 carbon atom in the *ortho*-naphthoiminoquino-

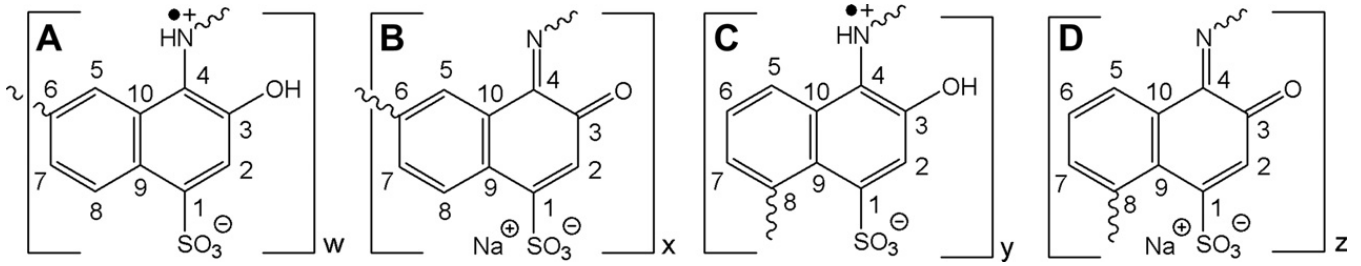

Scheme 6. The proposed structure of the poly(AHNSA-Na salt) with dominant structural units, where x > w, z > y, and w + x > y + z.

noid units (B, D). The disappearance of the peak at 111 ppm, assigned to the C4 carbon atom of the AHNSA, is another indication for the involvement of the aromatic amino group in coupling reactions.

3.8. ESR spectroscopy

The poly(AHNSA–Na salt) gives a strong asymmetrical ESR peak, Fig. 7, indicating the existence of paramagnetic state/unpaired electrons in the polymer [43]. The ESR *g* factor is determined to amount 2.0062.

3.9. Conductivity measurements

The conductivity of the poly(AHNSA–Na salt) is 8.4×10^{-7} S cm^{-1}. The acid doping of the poly(-AHNSA–Na salt) produces poly(AHNSA) with two orders of magnitude lower conductivity.

The PM3 RHF optimization of geometry revealed flip-flop stereochemistry of the poly (AHNSA–Na salt), caused by steric hindrance. Dihedral angles between adjacent AHNSA monomeric units approach 90° in a number of different coupling modes and redox forms. Polaronic forms resembling emeraldine salt of polyaniline, proved by ESR spectroscopy, are possible only for the oligomeric segments with N–C6 and N–C8 coupled AHNSA units. Steric hindrance is the main destabilizing factor for the existence of the poly(AHNSA–Na salt) polaronic forms, because their stability, based on delocalization of spin density through polymer chains, significantly decreases going from flattened to flip-flop structures. Consequently, only the AHNSA oligomers with exclusively N–C6 coupled AHNSA units can exist in a stable polaronic form.

Prevalence of the oligomeric, bipolaronic redox forms over polaronic forms is proposed as main reason for the observed semiconductivity.

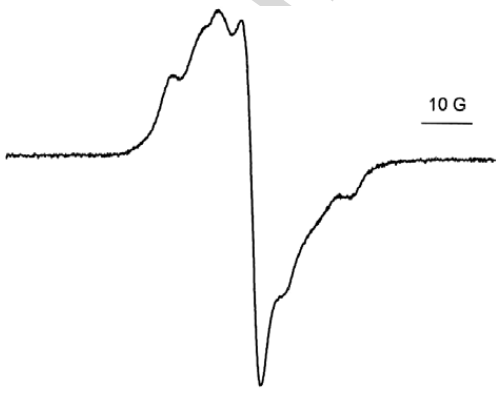

Fig. 7. The ESR spectrum of poly(AHNSA–Na salt).

3.10. Cyclic voltammetry

Electropolymerization products show electroactivity expressed on the final cyclovoltammetric (CV) curve by four anodic peaks at following potentials: −0.30 V (Ia), 0.16 V (IIa), 0.50 V (IIIa) and 0.80 V (IVa), as well as by four cathodic peak occurring at potentials: −0.60 V (Ic), −0.22 V (IIc), 0.26 V (IIIc) and 0.60 V (IVc) (Fig. 8).

The irreversible intensive oxidation peak at about 1.0 V is observed only at initial CV curve. It can be associated with monomer oxidation, similarly to the behavior usually observed for other aromatic amines [5]. A large cathodic current at potentials more negative than −0.5 V corresponds to the reduction of H^+ ions, released during the polymerization process [44]. Cyclovoltammetric peaks Ic/Ia and IIc/IIa are assigned to the redox processes of reduced/polaronic forms and polaronic/partly oxidized bipolaronic forms of the poly(AHNSA–Na salt), respectively, while peaks IIIc/IIIa and IVc/IVa could be attributed to the redox processes of partly oxidized/fully oxidized bipolaronic forms of the poly(AHNSA–Na salt) (Scheme 5).

hors personal copy

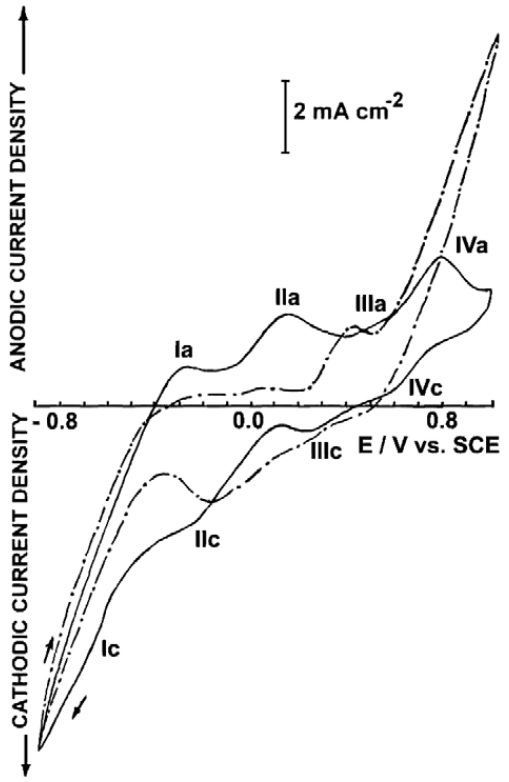

Fig. 8. The cyclic voltammograms of the reaction solution containing 0.084 mol dm^{-3} AHNSA–Na salt, recorded at the start of electropolymerization (–·–) (second cycle is shown) and after the reaction time of 10 h (—).

4. Conclusion

Despite the fact that the *para*- and both *ortho*-positions to the amino group of AHNSA–Na salt are occupied, the electrochemical oxidation of sodium 4-amino-3-hydroxynaphthalene-1-sulfonate results in water-soluble poly(AHNSA–Na salt) with molecular weight approaching a maximum value of ~6300. The GPC molecular weight distribution results suggest oligomeric products (8-mer to 12-mer) as dominant.

Data from FTIR spectroscopic study of substitution patterns on naphthalene and *ortho*-naphthoiminoquinonoid rings in the poly(AHNSA-Na salt), combined with ^{1}H and ^{13}C NMR spectroscopic investigation and theoretical PM3 calculations allow us to specify that N–C6 and N–C8 linkages prevailed in the structure of obtained polymerization products. UV–visible spectroscopy revealed that the structure of poly(AHNSA–Na salt) is a mixture of polaronic and bipolaronic redox forms, with prevalence of partly and fully oxidized bipolaronic forms. This is in accordance with Raman, FTIR, ^{1}H and ^{13}C NMR spectroscopic findings of *ortho*-naphthoiminoquinonoid and benzenoid presence in polymeric products. Cyclic voltammetry study confirms the complex redox behavior of the poly(AHNSA-Na salt).

Poly(AHNSA–Na salt) shows semiconductivity ($\sim 1 \times 10^{-6}$ S cm^{-1}) which originates from unpaired electrons (polaronic forms), as it was proved by ESR spectroscopy. This feature is in good correlation with mainly flip-flop stereochemistry of poly(-AHNSA-Na salt), as well as with its oligomeric and prevailing bipolaronic structure.

Acknowledgements

The authors wish to thank the Republic Serbia Ministry of Science and Environmental Protection (Contracts Nos. 142047 and 142010), the Grant Agency of the Academy of Sciences of the Czech Republic (A4050313 and A400500504) and the Ministry of Education, Youth and Sports of the Czech Republic (MSM 6046137307) for financial support.

The authors wish to thank Dr. Jaroslav Stejskal of Institute of Macromolecular Chemistry, Prague, for his valuable suggestions during the progress of this work.

References

[1] E.M. Genies, M. Lapkowski, Electrochim. Acta 32 (1987) 1223.
[2] T. Ohsaka, K. Hirabayashi, N. Oyama, Bull. Chem. Soc. Jpn. 59 (1986) 3423.
[3] S.S. Huang, J. Li, H.G. Lin, R.Q. Yu, Mikrochim. Acta 117 (1995) 145.
[4] G. Ćirić-Marjanović, B. Marjanović, V. Stamenković, Ž. Vitnik, V. Antić, I. Juranić, J. Serb. Chem. Soc. 67 (2002) 867.
[5] A.H. Arévalo, H. Fernández, J.J. Silber, L. Sereno, Electrochim. Acta 35 (1990) 741.
[6] N. Oyama, K. Hirabayashi, T. Ohsaka, Bull. Chem. Soc. Jpn. 59 (1986) 2071.
[7] H. Yang, F.-R. Fan, S-L. Yau, A.J. Bard, J. Electrochem. Soc. 139 (1992) 2182.
[8] S.-S. Huang, H.-G. Lin, R.-Q. Yu, Anal. Chim. Acta 262 (1992) 331.
[9] Y. Xu, Q. Xie, M. Hu, L. Nie, S. Yao, J. Electroanal. Chem. 389 (1995) 85.
[10] B.K. Schmitz, W.B. Euler, J. Electroanal. Chem. 399 (1995) 47.
[11] C.-Y. Chung, T.-C. Wen, A. Gopalan, Spectrochim. Acta Part A 60 (2004) 585.
[12] A. Meneguzzi, M.C. Pham, J.C. Lacroix, B. Piro, A. Adenier, C.A. Ferreira, P.C. Lacaze, J. Electrochem. Soc. 148 (2001) B121.
[13] A. Meneguzzi, C.A. Ferreira, M.C. Pham, M. Delamar, P.C. Lacaze, Electrochim. Acta 44 (1999) 2149.
[14] A. Nasalska, M. Skompska, J. Appl. Electrochem. 33 (2003) 113.

Authors personal copy

[15] S. Ito, K. Murata, Y. Asako, Nippon Shokubai Co., Ltd., US Patent 5,993,694, 1999.
[16] Y. Cao, P. Smith, A.J. Heeger, Synth. Met. 48 (1992) 91.
[17] G. Ćirić-Marjanović, N. Cvjetićanin, S. Mentus, J. Budinski-Simendić, I. Krakovsky, Polym. Bull. 50 (2003) 319.
[18] O.I. Aksimentyeva, Mol. Cryst. Liq. Cryst. 324 (1998) 125.
[19] A.R. Leach, Molecular Modelling Principles and Applications, Addison Wesley Longman, Essex, 1996.
[20] J.J.P. Stewart, J. Comput. Chem. 10 (1989) 209.
[21] J.J.P. Stewart, J. Comput. Chem. 10 (1989) 221.
[22] A. Klamt, G. Schüürmann, J. Chem. Soc. Perkin Trans. 2 (1993) 799.
[23] L.J. Bellamy, The Infra-red Spectra of Complex Molecules, Richard Clay and Company Ltd., Bungay Suffolk, 1962, pp. 65–84, 249–261.
[24] A.D. Cross, R.A. Jones, An Introduction to Practical Infrared Spectroscopy, Butterworths, London, 1969, pp. 76–79.
[25] J. Coates, in: R.A. Meyers (Ed.), Encyclopedia of Analytical Chemistry, Interpretation of Infrared Spectra, A Practical Approach, Wiley, Chichester, 2000, pp. 10815–10837.
[26] G. Socrates, Infrared and Raman Characteristic Group Frequencies, Wiley, New York, 2001, pp. 96, 157–167, 220–222.
[27] J. Tang, X. Jing, B. Wang, F. Wang, Synth. Met. 24 (1988) 231.
[28] M.I. Boyer, S. Quillard, E. Rebourt, G. Louarn, J.P. Buisson, A. Monkman, S. Lefrant, J. Phys. Chem. B 102 (1998) 7382.
[29] R.G.J. Miller, H.A. Willis, Infrared Structural Correlation Tables and Data Cards, Heyden and Son Limited, London, 1969.
[30] G. Ćirić-Marjanović, N. Cvjetićanin, S. Mentus, Spectrosc. Lett. 36 (1&2) (2003) 151.
[31] R.M. Silverstein, G.C. Bassler, T.C. Morrill, Spectrometric Identification of Organic Compounds, Wiley, New York, 1991, pp. 110–140.
[32] I. Sapurina, A.Yu. Osadchev, B.Z. Volchek, M. Trchová, A. Riede, J. Stejskal, Synth. Met. 129 (2002) 29.
[33] J.M. Kinyanjui, R. Harris-Burr, J.G. Wagner, N.R. Wijeratne, D.W. Hatchett, Macromolecules 37 (2004) 8745.
[34] M.C. Pham, B. Piro, E.A. Bazzaoui, M. Hedayatullah, J-C. Lacroix, P. Novák, O. Haas, Synth. Met. 92 (1998) 197.
[35] A. Petr, L. Dunsch, J. Phys. Chem. 100 (1996) 4867.
[36] G.S. Hammond, J. Am. Chem. Soc. 77 (1955) 334.
[37] H.W. Siesler, K. Holland-Moritz, Infrared and Raman Spectroscopy of PolymersPractical Spectroscopy, vol. 4, Marcel Dekker Inc., New York and Basel, 1980.
[38] G. Niaura, R. Mažeikiene, A. Malinauskas, Synth. Met. 145 (2004) 105.
[39] K. Berrada, S. Quillard, G. Louarn, S. Lefrant, Synth. Met. 69 (1995) 201.
[40] M.C. Bernard, A. Hugot-Le Goff, Synth. Met. 85 (1997) 1145.
[41] Lj. Arsov, K. Čolančeška, N. Petrovska, J. Serb. Chem. Soc. 63 (1998) 289.
[42] M. Sacak, U. Akbulut, D.N. Batchelder, Polymer 40 (1998) 21.
[43] R. Murugesan, E. Subramanian, Mater. Chem. Phys. 80 (2003) 731.
[44] N. Vettorazzi, J.J. Silber, L. Sereno, J. Electroanal. Chem. 125 (1981) 459.

Author's personal copy